RMetS
Royal Meteorological Society

Diurnally forced convergence lines in the Australian Tropics

Michael J. Reeder[a]*, Roger K. Smith[b], John R. Taylor[c], David J. Low[c], Sarah J. Arnup[a], Les Muir[d] and Gerald Thomsen[b]

[a]*School of Mathematical Sciences, Monash University, Clayton, Australia*
[b]*Meteorological Institute, University of Munich, Germany*
[c]*School of Physical, Environmental and Mathematical Sciences, University of New South Wales, Canberra, Australia*
[d]*Department of Geology and Geophysics, Yale University, USA*

*Correspondence to: M. J. Reeder, School of Mathematical Sciences, Monash University, Wellington Road, Clayton, Victoria 3800, Australia. E-mail: michael.reeder@monash.edu

Observations and analyses of low-level convergence lines over the Gulf of Carpentaria region of northeastern Australia made during the second and third Gulf Lines EXperiments (GLEX II and GLEX III) are reported.

During GLEX II, the initiation of the North Australian Cloud Line (NACL) was documented using a small autonomous aircraft and two Doppler sodars. NACLs are long convergence lines that form on the western side of northern Cape York Peninsula and are typically marked by a line of contiguous cumulus or cumulus congestus cloud. The observations show that the degree of asymmetry between west-coast and east-coast sea breezes (as characterized by the wind field) depends on the strength of the background easterlies, and that NACLs develop only when the background easterlies are sufficiently large (≥ 5 m s^{-1}).

GLEX III focused on morning glories, which are (mostly) southwestward-moving bore-like convergence lines that originate over the southern part of the gulf region. The field experiment involved Doppler sodar measurements as well as high-temporal-resolution data from operational automatic weather stations. The sodar measurements showed that undular bore-like morning glory cloud lines develop only when the background easterlies are sufficiently weak (≤ 10 m s^{-1}) and that strong bore-like morning glories develop when the background winds exceed about 10 m s^{-1}. If the background easterlies are too strong, no morning glories develop. Numerical simulations show that the structure of convergence line produced depends on the strength of the collision between the sea breezes from each side of the Cape York Peninsula, which in turn depends on the strength of the background easterlies. When the easterlies are weak (≤ 10 m s^{-1}), the sea breezes have similar depths and strengths, and their collision is relatively violent, whereas when the background easterlies are strong (> 10 m s^{-1}) the sea breezes have very different depths and strengths and their collision is comparatively benign. Copyright © 2012 Royal Meteorological Society

Key Words: bore; cloud lines; cold front; diurnal cycle; morning glory; sea breeze

Received 2 February 2012; Revised 26 June 2012; Accepted 11 July 2012; Published online in Wiley Online Library

Citation: Reeder MJ, Smith RK, Taylor JR, Low DJ, Arnup SJ, Muir L, Thomsen G. 2021. Diurnally forced convergence lines in the Australian Tropics. *Q. J. R. Meteorol. Soc.* DOI:10.1002/qj.2021

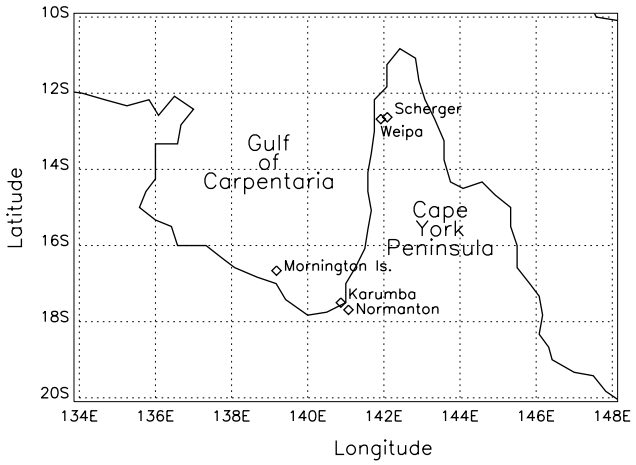

Figure 1. Map of northeastern Australia marking the places mentioned in the text. The abscissa is longitude in degrees and the ordinate is latitude in degrees.

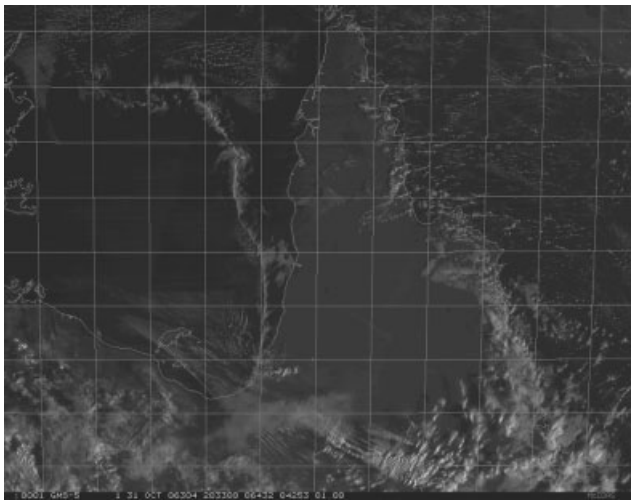

Figure 2. GMS visible satellite image, 0630 LST 31 November 2006.

1. Introduction

Convergence lines produced by the diurnal cycle of continental heating and cooling are thought to play an important role in the initiation and organization of clouds and convection in the Tropics. In the Gulf of Carpentaria region of northern Australia, three kinds of diurnally-forced convergence lines have been identified. (The locations referred to in the text are marked in Figure 1.) A review of these lines, including numerous references, can be found in Reeder and Smith (1998) and Weinzierl *et al.* (2007).

The first kind of convergence line is the North Australian Cloud Line (NACL), which forms on many days throughout the year. In the dry and transition seasons, NACLs are typically marked by a line of contiguous cumulus or cumulus congestus cloud, whereas in the wet season they generally comprise cumulonimbi. NACLs are often more than 500 km long, stretching the length of the Gulf of Carpentaria from the southeast to the northwest. The Geostationary Meteorological Satellite (GMS) visible satellite image at 0630 LST (Local Standard Time: LST = UTC + 10 h) 31 November 2006 (Figure 2) shows a distinct NACL just off the west coast of the Cape York Peninsula and aligned roughly north–south.

The second kind of convergence line gives rise to the morning glory, which refers to one or a series of low-level cloud lines that are observed predominantly during the late dry season (September–November) in the southeastern part of the Gulf and the southwestern part of the Cape York Peninsula. Although not all disturbances are marked by cloud, the term 'morning glory' is used here to describe the convergence line also when it is cloud free. Dynamically, the morning glory convergence line is a propagating bore, which is sometimes undular (see, for example, Clarke *et al.*, 1981; Menhofer *et al.*1997a). The defining feature of a bore is that the pressure rises sharply with its passage and remains high thereafter. In an undular bore, the leading pressure jump is followed by a train of large-amplitude waves in the pressure trace with the time–mean pressure higher than that before the jump.

Morning glories are known to propagate from three preferred directions: from the northeast, the south and the southeast. Those from the northeast–northeasterly morning glories–are closely connected to NACLs as both originate over the Cape York Peninsula from the interaction of the east-coast and west-coast sea breezes (Clarke *et al.*, 1981; Clarke, 1983a, 1983b, 1984; Noonan and Smith, 1986, 1987; Thomsen and Smith, 2006). Morning glories that propagate from the south are generated by cold fronts as the latter strengthen and accelerate overnight (Smith *et al.*, 1995; Deslandes *et al.*, 1999; Reeder *et al.*, 2000; Thomsen *et al.*, 2009). The origin of southeasterly morning glories is less well understood than that of northeasterly and southerly morning glories, although there is much evidence to suggest that they are linked to subtropical cold fronts and/or to the nocturnal intensification of the dry line (Smith *et al.*, 1995, 2006; Reeder *et al.*, 1995; Reeder *et al.*, 2000; Thomsen and Smith, 2006). In addition to the NACL, Figure 2 shows a northeasterly morning glory in the southeastern part of the Gulf marked by a series of cloud lines aligned northwest–southeast. On occasion, NACLs and northeasterly morning glories do occur simultaneously as both are produced by the sea breeze that form along the east coast of the Cape York Peninsula (as is discussed in detail later in the paper).

The dry line is the third kind of diurnally-forced convergence line in the Gulf region and it, too, is occasionally the focus of deep convection. While not the focus of the present study, the dry line is perhaps the dominant surface feature of the northern Australian region (Arnup and Reeder, 2007, 2009).

The first major field experiment to study the morning glory was conducted in the late dry season of 1979, the findings from which were presented by Clarke *et al.*, (1981). In the years that followed, further field experiments were carried out, including one designed specifically to investigate the NACL, which was performed in late 1986. As a result of these experiments and supporting numerical simulations, the basic structure of both types of disturbance were identified. The results of these studies are summarized by Reeder and Smith (1998).

The availability of significantly improved measurement capabilities towards the end of the 20th century, as well as improved numerical models, stimulated further studies into both types of convergence lines. A preliminary numerical study by Jackson *et al.* (2002) pointed to the possibility that these lines might be predictable using operational mesoscale models. This study led to the organization of the Gulf

Lines field Experiment (GLEX).* The first phase–GLEX I–was carried out in the late dry season of 2002 with the main focus of documenting NACLs and southerly morning glories and systematically investigating their predictability. The results of this experiment were reported in a series of papers by Goler *et al.* (2006), Smith *et al.* (2006), Thomsen and Smith (2006) and Weinzierl *et al.* (2007).

The present paper presents the results of two subsequent field experiments–GLEX II and GLEX III–which were conducted during 2005 and 2006, respectively. The GLEX II experiment was designed to focus on NACLs in the northern gulf region, while GLEX III focused on late dry-season morning glories in the southeastern corner of the Gulf.

The paper is structured as follows. Section 2 outlines the two experiments GLEX II and GLEX III and the instruments deployed. The section summarizes also the main characteristics and configurations of the two models used in the subsequent interpretation of the observations, viz. the Australian Bureau of Meteorology's Limited area Assimilation and Prediction System (LAPS) and the Pennsylvania State University–National Center for Atmospheric Research fifth-generation Mesoscale Model (MM5; version 3.6). Section 3 sets the scene for later composite analyses with an analysis of the observations taken during GLEX II on 13–14 December 2005. Composites of the sodar measurements and 3 h forecasts for both experiments, based on LAPS, are described in sections 4 and 5. Time series of surface pressure over the southern Gulf are presented also in section 5. The observations are synthesized in section 6, where they are related to existing theoretical and modelling results. The ideas raised in section 6 are explored further in section 7 with the aid of the two simulations using MM5. In particular, how the collision between the east-coast and west-cost sea breezes changes with changing background easterlies is examined, along with how these differences shape the structure of the resulting NACL and morning glory. The conclusions are summarised in section 8.

2. Field experiments and models

The GLEX II experiment ran from 18 November to 18 December 2005 and observations were made in the vicinity of Weipa, a town located on the northwestern side of Cape York Peninsula. At this latitude, Cape York Peninsula is approximately 160 km wide, bounded on the east coast by the Coral Sea and on the west coast by the Gulf of Carpentaria. The GLEX III experiment ran from 17 September to 7 November 2006 with observations focused on the southeastern corner of the Gulf region. The instruments deployed for these experiments and the models used in their interpretation are described below.

2.1. Sodar

During GLEX II, the University of New South Wales, Canberra, deployed a medium-frequency Doppler sodar at the Bureau of Meteorology site at Weipa Airport (12°40.7′S, 141°55.5′E) and another at the nearby Scherger base of the Royal Australian Air Force (12°37.4′S, 142°5.2′E). The Scherger sodar was located approximately 4 km north and 19 km east of that at Weipa. During GLEX III, one sodar was located at the Normanton Racetrack (17°41.3′S, 141°4.0′E), which is about 32 km inland from the southern Gulf coast. The sodars were three-axis, single-transducer, dish antenna type operating at 1.852 kHz. The first level sampled was centred at 50 m and levels were spaced at 30 m intervals. For the full period of the experiments, both raw Doppler spectra and radial winds from real-time processing were logged on the sodar controller computer. The sodars gave reliable wind profiles up 500 m in most conditions, providing detailed time–height cross-sections of the winds in the boundary layer. The analysis presented here uses the real-time wind data averaged into 30 min blocks.

2.2. Aerosonde

The Aerosonde is a miniature robotic aircraft developed over the past decade for meteorological and environmental reconnaissance and atmospheric measurement over oceanic and remote areas. The aircraft weighs less than 15 kg and can fly autonomous missions of over 30 h. The instruments on the Aerosonde measured wind speed, wind direction, temperature, pressure and humidity. During GLEX II, the Aerosonde was launched from Weipa airport. Unfortunately, it was dogged by a series of mechanical and electronic faults, with the result that far fewer successful missions than planned were possible. The results from one successful flight on 13–14 December 2005 are reported here.

2.3. Mornington Island Automatic Weather Station

For GLEX III, the Bureau of Meteorology upgraded its automatic weather stations in the region to record data with a temporal resolution of 1 min. Here, use is made of the time series at Mornington Island, which lies in the southeastern part of the Gulf of Carpentaria (16°30.0′S, 139°30.0′E).

2.4. LAPS

The large-scale environment in which the sodar measurements were taken is characterized using 3 h forecasts from LAPS, a combined numerical forecast model and objective analysis scheme with a horizontal resolution of 0.375° (which is around 40 km resolution in the Gulf region) (Puri *et al.*, 1998). Before discussing the forecasts for the experimental period, it is appropriate to summarize briefly the main features of LAPS. The forecast model is based on the hydrostatic primitive equations in σ-coordinates, where $\sigma = p/p_s$, p is pressure and p_s is the surface pressure. LAPS includes a prognostic equation for the surface temperature, as well as parametrizations of boundary-layer physics, large-scale and convective precipitation, and radiation. Every 6 h, LAPS assimilates surface synoptic measurements, ship and drifting buoy reports, radiosonde and upper-level wind observations, satellite sounding data from the TIROS Operational Vertical Sounder, Geostationary Meteorological Satellite (GMS) cloud-drift winds and single-level winds from aircraft reports. The initial conditions are interpolated from the Bureau of Meteorology's lower-resolution Global ASsimilation and Prediction system (GASP), and consequently are relatively featureless.

*Morning glory convergence lines and NACLs are sometimes known simply as gulf lines.

2.5. MM5

Some of the ideas to emerge from the analysis of the observations are investigated further in two simulations using the MM5 model (Dudhia, 1993; Grell *et al.*, 1995). The main features of MM5 and the configuration used here are briefly as follows. The model is non-hydrostatic and uses a finite difference approximation to the governing equations. The calculations described are made on two nested, horizontal domains. The outer domain has 221 × 221 grid points with a horizontal grid spacing of 9 km and the inner domain has 400 × 400 points with a horizontal grid spacing of 3 km. The time step is 27 s for the outer domain and 9 s for the inner domain.

The land use and orography are taken from the US Geological Survey dataset included in the standard MM5 modelling configuration. The cumulus parametrization scheme is not used in either domain. All domains use the boundary-layer scheme as implemented in the National Centers for Environmental Prediction (NCEP) Medium Range Forecast (MRF) system by Hong and Pan (1996). Thomsen and Smith (2008) showed that this scheme was the best of those available in MM5 for predicting Gulf convergence lines. The Dudhia scheme (Dudhia, 1989) is chosen to represent explicit moisture conversions and a bucket scheme is used for the soil moisture budget. The radiation scheme used is that developed by Stephens (1978), Garand (1983) and Stephens *et al.* (1984). A gravity wave radiation scheme is applied at the upper boundary to inhibit the reflection of wave energy from the model top.

The initial conditions and outer boundary conditions are taken from the European Centre for Medium Range Weather Forecasts operational analyses. These data have a horizontal resolution of 0.25° (which is about 27 km resolution in the Gulf region). The vertical coordinate is $\sigma = (p - p_t)/(p_s - p_t)$, where p is the pressure, p_s is the surface pressure and p_t the pressure at the upper boundary, set here to 100 mb. There are 23 σ-levels in total, with the lowest 15 levels located at the approximate heights, 0, 40, 80, 150, 230, 300, 380, 540, 700, 870, 1200, 1550, 1900, 2300 and 2750 m, giving relatively high resolution in the boundary layer. Further details of the model can be found in Grell *et al.* (1995). The numerical integrations for Experiment 1 and Experiment 2 begin at 1000 LST on 19 September and 1000 LST on 24 September, respectively.

3. The event of 13–14 December 2005

An analysis of the observations taken on 13–14 December 2005 is described now. This particular day was chosen as it was the day on which the data from the Aerosonde was most complete. Meteorologically, the day was typical of the period.

The GMS visible satellite image at 0630 LST 14 December (Figure 3) shows a weak, zigzag-shaped NACL aligned roughly northnorthwest to southsoutheast over the Gulf and a morning glory in the southeastern part of the Gulf marked by a series of curved cloud lines. Judging from the alignment of the cloud lines, the morning glory appears to have propagated from the southeast. (Southeasterly morning glories have received relatively little attention in the literature. A recent discussion on what is known on this class of disturbances is given by Smith *et al.*, 2006.)

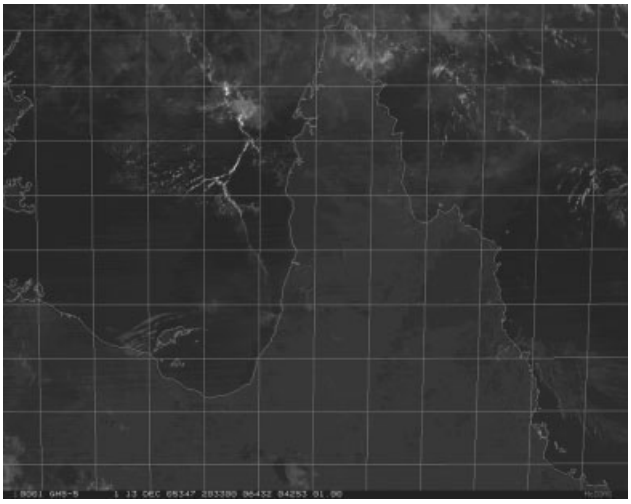

Figure 3. GMS visible satellite image, 0630 LST 14 December 2005.

Figure 4 shows time–height cross sections of the horizontal wind from the sodars at Weipa and Scherger for a 24 h period commencing 1200 LST on 13 December. At about 1500 LST, the winds at Weipa change from easterly to westerly, marking the arrival of the west-coast sea breeze. Thereafter, they strengthen, reaching a maximum at a height of approximately 200 m at 1700 LST. In contrast, the westerlies do not arrive at Scherger until about 1700 LST as it is about 19 km inland from Weipa. Likewise, the east-coast sea breeze, as marked by the return to easterly flow, arrives at Scherger at around 2130 LST, but its arrival is delayed at Weipa until 2230 LST. At both Weipa and Scherger, a low-level easterly forms in the early hours of the morning. At both sites also, strong easterlies develop at a height of about 300 m at around 0200–0300 LST and subsequently accelerate through a deeper layer until about 0900 LST. That the maximum wind speeds are high above the ground in the early hours of the morning is presumably due to the weaker vertical transfer of momentum at night. The structure and nocturnal evolution of the wind field is similar to that reported by May (1995) in a study based mainly on wind profiler observations taken at Mt Isa in northeastern Australia (20.7°S, 139.5°E). May found that, on average, the low-level winds peaked at around 0700 LST at a height of about 600 m, and that this jet dissipated at around 0900 LST with the onset of deep (dry) convective mixing.

The dew-point and zonal (west to east) component of the wind from the Aerosonde flight of 13–14 December 2005 are plotted in Figure 5. The flight path was predominantly east–west at three different heights; 180, 290 and 400 m. The flight data are broken into segments and plotted as a function of the east–west distance from Weipa airport rather than time. The segments are ordered in the figure according to their midpoint time. The most prominent feature in the observations is the west-coast sea breeze, which is marked as 1 (in both Figures 4 and 5). In Figure 5, both the wind change and fall in dew temperature point are sharp and strong, being approximately 10 m s^{-1} and 8 K respectively. The west-coast sea breeze is strongest in the lowest-level segment (180 m high) and propagates inland with a mean speed of 2.3 m s^{-1}. There is a wind change from westerly to northerly at about 2300 LST, but little change in dew-point. This change is marked as 2. In the same data segment, but further to the east, the east-coast sea breeze is marked as 3.

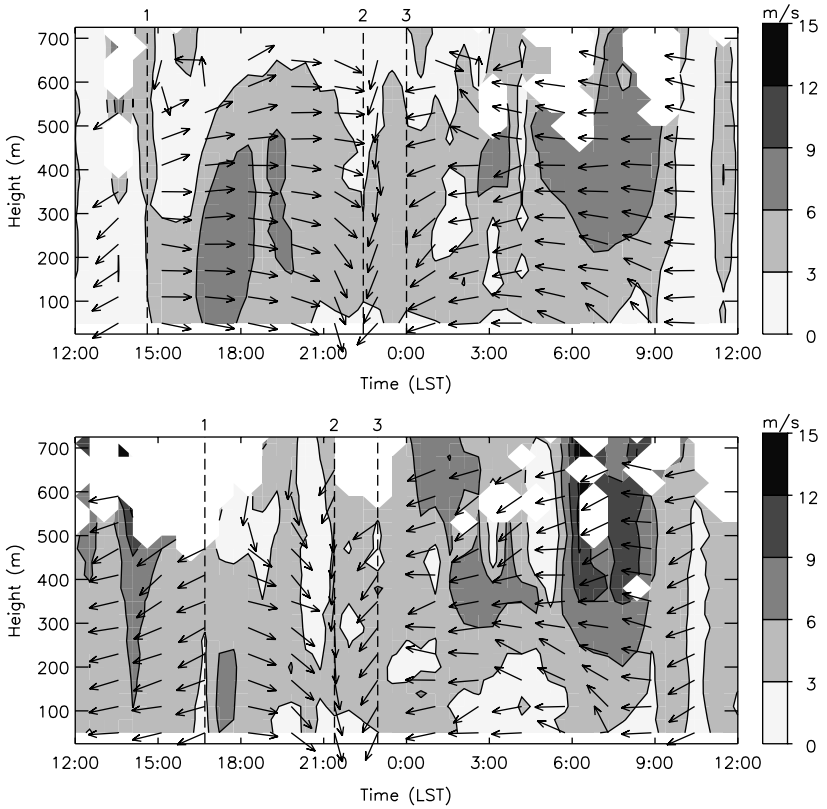

Figure 4. Horizontal winds for the period 13–14 December 2005. Top: Weipa; bottom: Scherger. Vectors indicate the wind direction and the shading shows the magnitude of the wind. The data are averaged over 30 min intervals. The numbers on the figures mark the corresponding features in Figure 5. The white regions in the plot indicate no data.

The east-coast sea breeze is accompanied by a marked shift to easterlies and a further fall in the dew-point of 1–2 K. This change subsequently propagates westwards at an average speed of 4.4 m s^{-1}.

4. GLEX II: Composite observations in the northeastern Gulf region

Recall that GLEX II was centred on Weipa on the northwestern side of the Gulf of Carpentaria and was dedicated to the observation of dry and transition-season NACLs.

Figure 6 shows composite time–height sections of the horizontal wind components from the sodar at Weipa. These composites are constructed as follows. First, whether or not there is an NACL is determined by visually inspecting the infrared (IR) GMS imagery. There are only 4 days on which there is no NACL and these are used to construct the first composite, shown in the top panel of Figure 6. Second, those days on which an NACL forms are composited according to the speed of the NACL. Those days on which the NACL is east of 140°E at 0630 LST are assigned to the second composite, shown in the middle panel of Figure 6, whereas those to the west of the longitude are assigned to the third composite, shown in the bottom panel of Figure 6. The number of days assigned to the second and third composites are 7 and 13 respectively. The same days assigned to each of the three groups are used to composite the horizontal wind components from the sodar at Scherger (Figure 7). The sodar observations taken on 13–14 December and discussed in section 3 are included in the second composite.

There is a strong connection between the composite and the strength of the easterlies behind the NACL. For each member of the first composite (top panel), the maximum easterly in the section between 0000 and 0900 LST is less than 5 m s^{-1}; the maximum easterly lies approximately between 5 and 10 m s^{-1} for each member of the second composite (middle panel); and the maximum easterly exceeds 10 m s^{-1} on each of the days in the third composite (bottom panel).

In the first composite of the winds from the Weipa sodar (Figure 6, top panel), comprising the days without NACLs, the winds between about 1200 and 2100 LST are westerly, which is onshore. The maximum westerly wind occurs around 1600 LST at a height of about 200 m and signals the onset of the west-coast sea breeze. Above about 300–400 m, the composite winds remain westerly throughout the night, although below this height weak easterlies develop after about 0100 LST. At the Scherger sodar, the winds change from easterly to westerly a little later at about 1430 LST (Figure 7, top panel), and the westerlies are strongest and deepest at about 1700 LST. After about 2000 LST the westerlies weaken significantly, becoming easterly at the lowest levels around 0200 LST. Between about 0600 and 1000 LST the easterlies strengthen markedly, particularly in the upper 200 m of the plot. Although a maximum appears in each of the three composites of the Scherger sodar winds and in Figure 4 at a similar time and location, it is sharpest in the first composite. However, as the composite comprises only 4 days, one needs to be a little cautious in interpreting Figure 7 (top panel), even though it is representative of the individual days. Around 0900 LST the winds weaken as the surface warms and the mixed layer deepens.

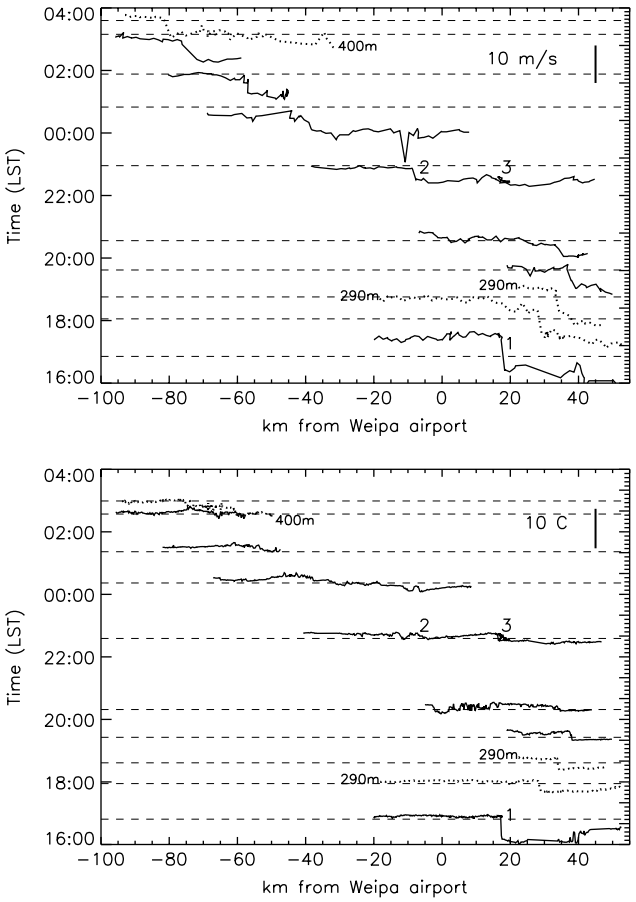

Figure 5. Segments of the Aerosonde observations from 13 to 14 December 2005. The abscissa represents the east–west distance from Weipa airport. The data segments are arranged with time running upwards and the ordinate marks the midpoint time for each data segment. Top: zonal component of the wind. The tick marks on the right-hand ordinate are 1 m s^{-1}. Bottom: dew-point. The tick marks on the right-hand ordinate are 1 °C. Solid lines indicate 180 m, whereas dotted lines indicate 290 m or 400 m. The numbers on the figures mark the corresponding features in Figure 4.

In the second Weipa sodar wind composite (Figure 6, middle panel), the winds change from southerly to westerly around 1330 LST, with the maximum westerly at around 1700 LST. The onset of the sea breeze is delayed by about an hour compared with the top panel of Figure 6 because of the stronger environmental easterlies. For the same reason, the easterlies arrive at Weipa at around 0000 LST, which is about an hour earlier than in the top panel of Figure 6. In contrast, a relatively strong low-level easterly flow with a maximum at about 200 m develops through the early hours of the morning. In the mid morning a southerly flow is re-established. In the second Scherger composite (Figure 7, middle panel), the westerlies arrive later and the maximum is closer to the surface at approximately 200 m. The easterlies arrive earlier than in the top panel of Figure 7, with a low-level jet developing below about 400 m. An NACL formed on every day in this composite.

In the third Weipa sodar wind composite (Figure 6, bottom panel), the afternoon westerlies are weaker, shallower and arrive later in the afternoon than in the middle panel of Figure 6. The easterlies arrive at Weipa at around 2130 LST and strengthen throughout the night. Unlike the middle panel of Figure 6, the easterlies increase with height. Easterlies dominate the composite at Scherger (Figure 7, bottom panel), with the strongest flow occurring shortly after sunrise. Weak westerlies are confined to the interval between 1700 and 2100 LST. An NACL formed also on each day comprising this composite.

Composites of the LAPS 3 h forecasts valid at 1800 LST and 0600 LST are shown in Figure 8. Each composite comprises the same days used to construct Figure 6. At the resolution of the LAPS 3 h forecasts, the west-coast sea-breeze circulation is marked by an area of reduced easterly winds just offshore of the west coast, in addition to convergence along the coast lines and offshore divergence (Figure 8, left column). On the eastern side of Cape York Peninsula, the sea breeze circulation strengthens the synoptic southeasterly onshore flow. As a result of turbulent mixing, the leading edge of the east-coast sea breeze is less pronounced than that of the west-coast sea breeze. As the background easterlies increase, this leading edge penetrates further inland. Twelve hours later, following the interaction of the east-coast and west-coast sea breezes, a well-defined convergence line lies across the gulf and southern part of the peninsula in the composite with the strongest background easterlies (Figure 8, bottom right panel). This line corresponds to the NACL. In contrast, there is no NACL in the composite with the weakest background easterlies (Figure 8, top right panel).

The intermediate composite (Figure 8, middle right panel) shows two distinct strips of elevated convergence. The easternmost strip is the model representation of the NACL, while the westernmost strip is probably the model representation of the morning glory. The role of the background easterlies in the formation of the morning glory will be addressed later in section 5.

The convergence lines in the second and third composites are accompanied by a weak potential temperature gradient with potentially cooler air to the east. Although not shown here, this cooler air mass forms over the peninsula overnight as the surface cools radiatively and is subsequently advected offshore by the strengthening easterlies.

5. GLEX III: Composite of observations in the southeastern Gulf region

In contrast to GLEX II, the subsequent experiment–GLEX III–focused on morning glory convergence lines. Therefore, GLEX III was centred on Normanton in the southeastern corner of the Gulf of Carpentaria.

Figure 9 shows composite time–height sections of the horizontal wind components from the sodar at Normanton. These composites are based on the maximum easterly component of the wind in the section and the detection of a pressure jump downstream at Mornington Island. These pressure jumps are surface signatures of the morning glories. The top panel shows the composite of all days for which the maximum easterly is less than 10 m s^{-1} and a pressure jump of at least 0.3 hPa in 3 min is detected downstream. The middle panel shows all days for which the maximum easterly exceeds 10 m s^{-1} and a pressure jump is detected downstream. The bottom panel shows the composite of those days for which no morning glory (i.e. pressure jump) is detected downstream. The three composites comprise 3, 14 and 19 days, respectively.

The first composite is shown in Figure 9 (top panel). A degree of caution is necessary in interpreting this composite as it comprises only 3 days. The winds at Normanton are westerly through the depth of the section for most of the afternoon and evening. These westerlies strengthen in the

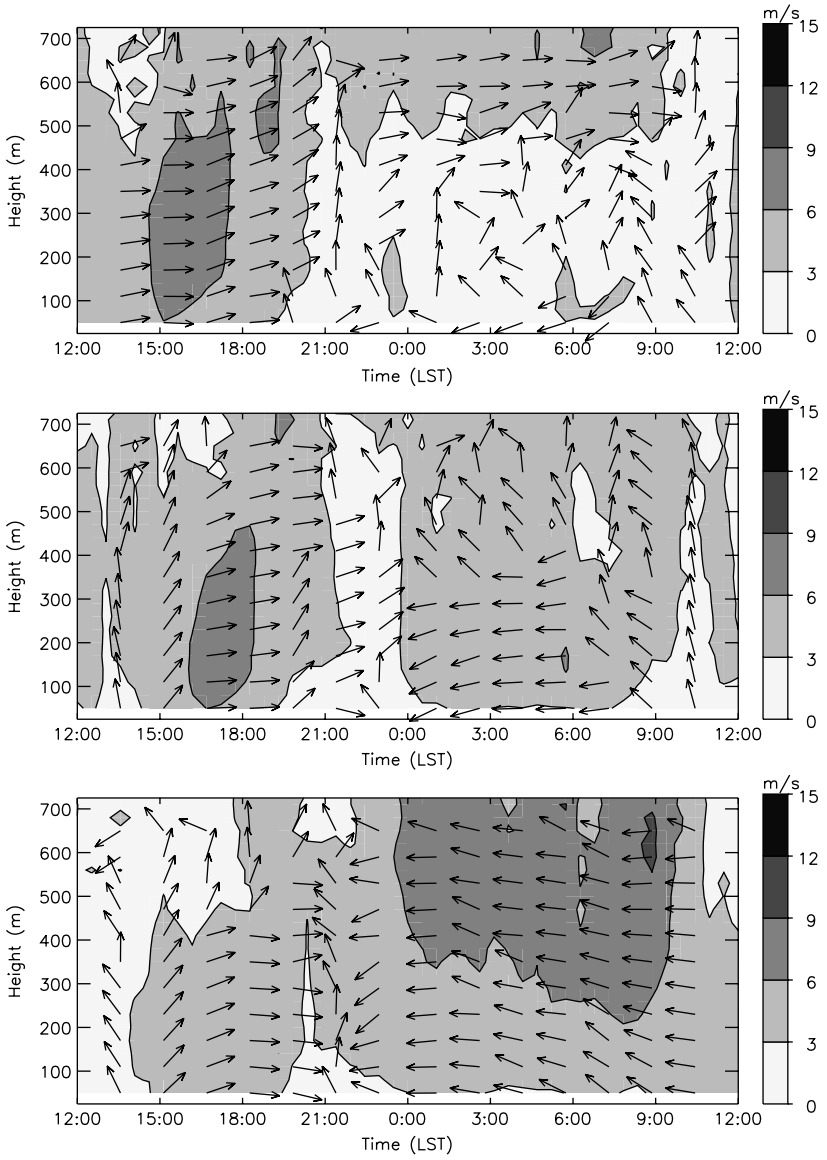

Figure 6. Composite horizontal winds from the Weipa sodar. Top: days without cloud lines. Middle: slow-moving cloud lines. Bottom: fast-moving cloud lines. Vectors indicate the wind direction and the shading shows the magnitude of the wind. The data are averaged over 30 min intervals.

evening, reaching a local maximum at a height of about 200 m at 2100 LST. From around midnight, the winds above 300 m progressively back and become southerly, whereas below 300 m a low-level westerly develops. This low-level wind attains a maximum just before the arrival of a deep easterly wind surge at 0600 LST. The second composite is shown in Figure 9 (middle panel) and, unlike that in the first composite, the winds are predominantly southerly prior to about 1800 LST. After this time a strong westerly develops with a maximum at 200 m at 2100 LST, similar to that in the first composite. In contrast to the first composite, however, a strong and deep easterly surge arrives at Normanton at about 0300 LST and persists until about 0900 LST. The third composite is shown in Figure 9 (bottom panel). The main differences between this and the previous composite are that the flow is easterly prior to about 1630 LST, the late evening westerly is weaker, and the easterly wind surge is stronger and arrives earlier.

The individual pressure time series from Mornington Island are sorted into the same three groups and plotted in Figure 10. The most striking aspect of the figure is that the pressure jumps that develop on days comprising the first composite (Figure 10, top panel) is strikingly different from those comprising the second composite (Figure 10, middle panel). In Figure 10 (top panel) the pressure jumps have the appearance of amplitude-ordered solitary waves,[†] whereas in Figure 10 (middle panel) the jumps are bore-like. (Note also that the top time series in Figure 10 from 25 September shows two families of morning glories. The first is a southerly morning glory generated by a cold front to the south, whereas the second is a more common northeasterly morning glory generated from the collision of sea breezes

[†]Theoretical descriptions of morning glory propagation have been developed within the framework of the weakly nonlinear wave theory. For example, see the review by Christie (1992). These theories consider long internal gravity waves propagating on a shallow stable layer with a deep fluid above, and assume the wave amplitude is small compared with the depth of the stable layer. Starting from smooth initial conditions, these weakly nonlinear theories predict the asymptotic development of a family of solitary waves. Moreover, as the phase speed of these waves increases with increasing amplitude, they are ordered according to their amplitude.

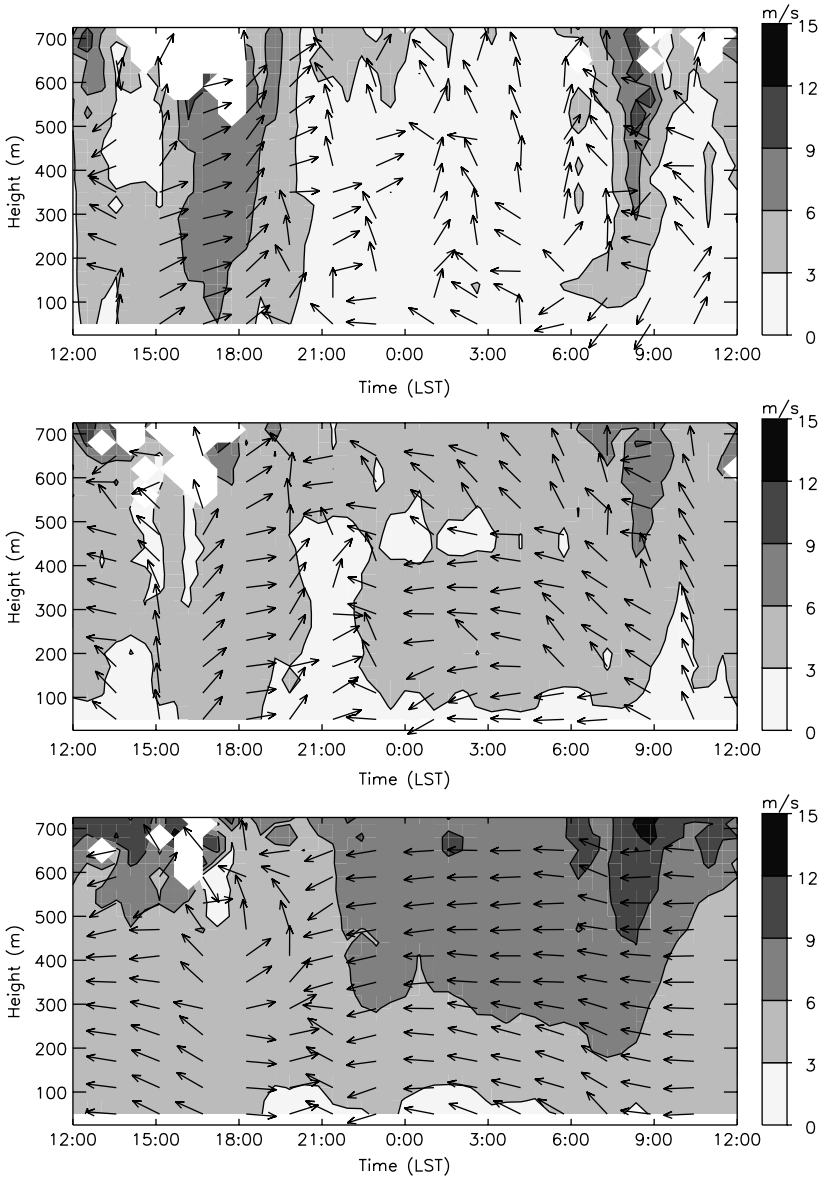

Figure 7. Composite horizontal winds from the Scherger sodar. Top: days without cloud lines. Middle: slow-moving cloud lines. Bottom: fast-moving cloud lines. Vectors indicate the wind direction and the shading shows the magnitude of the wind. The data are averaged over 30 min intervals. The white regions in the plot indicate no data.

over the Cape York Peninsula.) By construction, there are no significant pressure jumps in the third composite (Figure 10, bottom panel).

As in section 4, the large-scale environment is characterized by composites of the LAPS 3 h forecasts valid at 1800 LST and 0600 LST. Each composite shown in Figure 11 comprises the same days used to construct Figure 10. At 1800 LST (left-hand column) the environmental winds are not very different in each of the composites, with the exception of the area around Normanton in the southeastern corner of the gulf. In this region, the winds strengthen from the bottom panel to the top panel. At 0600 LST, the first and second composites show broad convergence lines over the gulf, which are the model representations of the morning glory. In contrast, the convergence line in the third composite is less well defined. Note also that the winds are stronger and the potential temperature contrast across the southern part of the convergence line is larger in the second and third composites compared with the first.

6. Discussion

The composite time–height sections of the horizontal component of the wind at Weipa and Scherger (Figures 6 and 7) show that the degree of asymmetry between west-coast and east-coast sea breezes (as characterized by the wind field alone) depends on the strength of the background easterlies. In light easterly flow (less than 5 $\mathrm{m\,s^{-1}}$) the onshore flow associated with the west-coast sea breeze is relatively strong and deep, whereas in strong easterly flow (greater than 10 $\mathrm{m\,s^{-1}}$) the onshore flow is relatively weak and shallow. These conclusions are consistent with the idealized large eddy simulations of interacting sea breezes reported by Goler and Reeder (2004), which showed that the depth of the west-coast sea breeze decreased with increasing background easterly flow.

The composite sections (Figures 6 and 7) and composite analyses (Figure 8) showed also that NACLs form only when the background easterlies are sufficiently strong and that they are accompanied by a weak low-level potential temperature

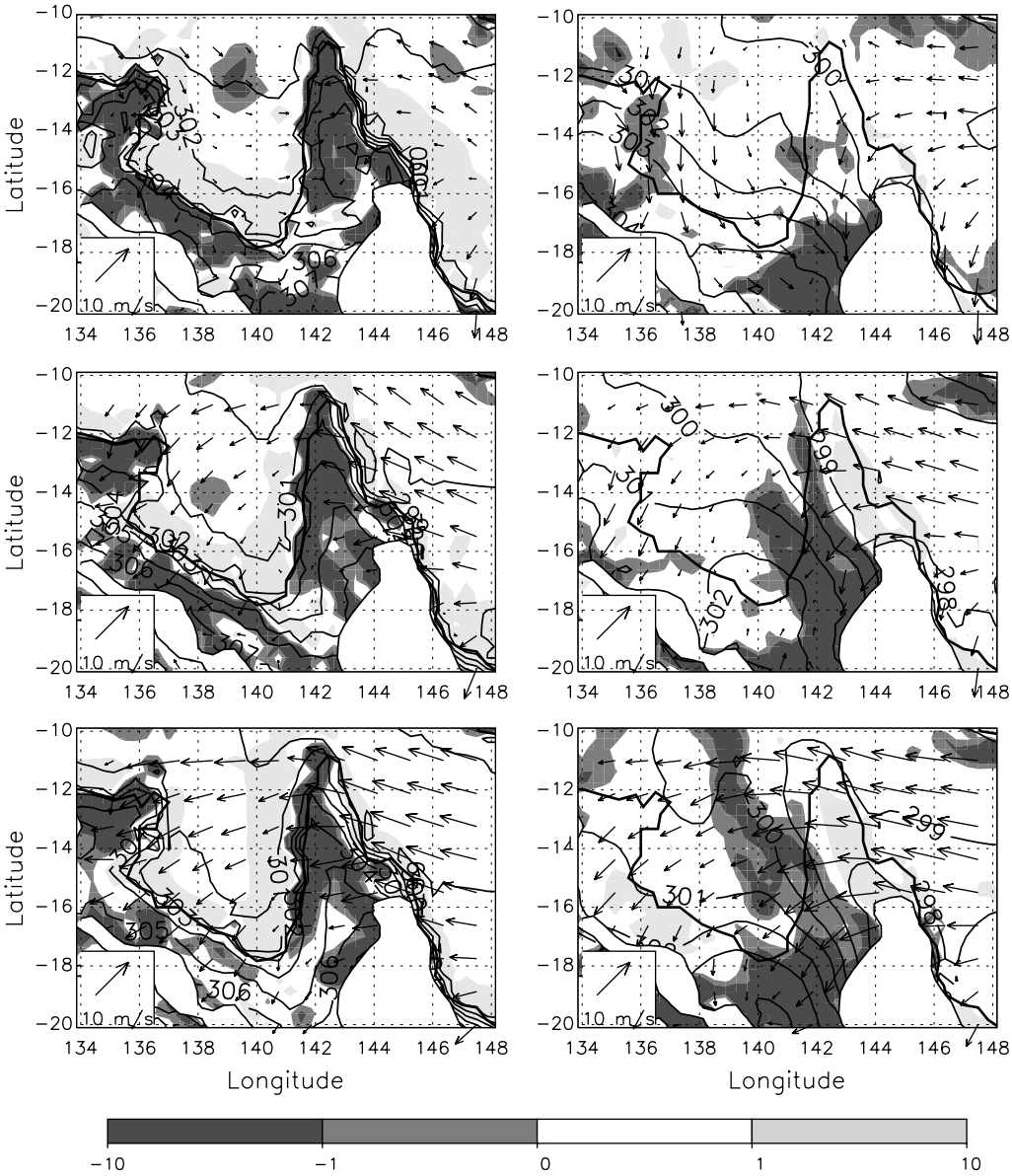

Figure 8. Composite LAPS 3 h forecasts at 950 mb showing convergence, horizontal winds and virtual temperature. Shading indicates divergence with units $\times 10^{-5}\,s^{-1}$. The contour interval for virtual temperature is 1 K. Top row: days without cloud lines. Middle row: days with slow-moving cloud lines. Bottom row: days with fast-moving cloud lines. Left column: 1800 LST. Right column: 0600 LST. The blank areas enclosed with a solid dark line indicate topography above 250 m.

gradient. This result is consistent with the observational and modelling work from GLEX I. Goler *et al.* (2006) found that the NACL develops at the leading edge of a weak gravity current, referred to as a land breeze by these authors, which moves westwards from Cape York Peninsula as the west-coast sea breeze decays. Strong easterly flow was found behind the NACL, with much weaker easterlies ahead of it. In numerical simulations, Goler *et al.* found that this land breeze was accompanied by convergence and upward motion at the leading edge of the weak low-level cold pool, leading to the development of cloud. Presumably, NACLs require relatively strong background easterlies because such a flow produces stronger low-level cold advection and hence stronger temperature gradients at the leading edge of the land breeze.

The composite time–height sections at Normanton (Figure 9) and the pressure time series from Mornington Island (Figure 10) suggest that amplitude-ordered solitary waves develop downstream if the maximum easterly flow is less than about 10 $m\,s^{-1}$. In contrast, a single bore-like jump forms downstream in stronger easterlies. However, if the background flow is greater than about 15 $m\,s^{-1}$, no pressure jump develops. Taken together, the observations from GLEX II and GLEX III suggest that strong easterlies favour the formation of the NACL, whereas weak easterlies favour the formation of the morning glory.

The mechanisms controlling how the morning glory depends on the strength of the background easterlies are probably more subtle than those controlling the NACL. This is because the strength of the background easterlies affects both the strength of the collision between the east-coast and west-coast sea breezes from which the morning glory evolves and the properties of the structure of the waveguide on which it subsequently propagates.

First consider the effect of the background flow on the collision. As shown by Goler and Reeder (2004), weak or zero background flows produce relatively symmetric sea breezes. The collision between the two symmetric sea breezes is

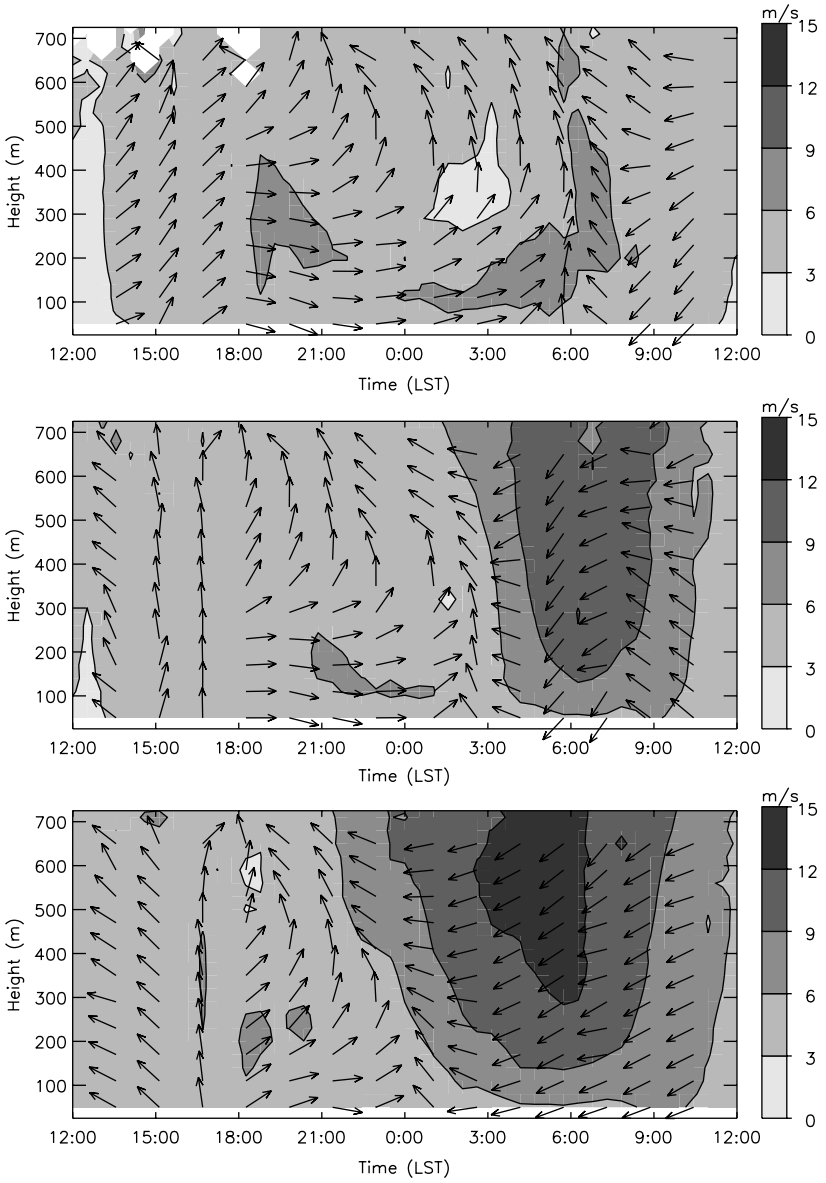

Figure 9. Composite horizontal winds from the Normanton sodar. Top: easterlies < 10 m s^{-1}. Days with solitary wave-like morning glories. Middle: easterlies > 10 m s^{-1}. Days with jump-like morning glories. Bottom: Days without morning glories. Vectors indicate the wind direction and the shading shows the magnitude of the wind. The data are averaged over 30 min intervals.

relatively strong, thrusting cold air violently upwards. Two bores emerge from this initial disturbance, propagating in opposite directions. The leading edges of the disturbances subsequently separate into a train of solitary waves (see, for example, Goler and Reeder's Figure 12.) Noonan and Smith (1987) and Thomsen and Smith (2006) have also identified this kind of strong collision as the mechanism by which morning glories are generated in their numerical simulations. In contrast, strong background flows produce highly asymmetric sea breezes, which do not collide violently. Instead, the east-coast sea breeze surmounts the west-coast sea breeze as its leading edge is locally more buoyant. Subsequently, solitary waves can be generated resonantly if the speed of the east-coast sea breeze matches the phase speed of the small-amplitude gravity waves on the layer of cold air that feeds the west-coast sea breeze (see, for example, Goler and Reeder's Figure 5). Resonance is not possible when the background flow is too strong as the speed of the east-coast sea breeze and the small-amplitude waves are too dissimilar. Indeed, Goler and Reeder found that no waves developed in their simulations when the easterlies exceeded 10 m s^{-1}.

Consider now the effect of the background easterlies on the medium through which the morning glory propagates. Although morning glory waves have large amplitude, linear theory has been used to describe, at least qualitatively, the structure of the waveguide on which they propagate (e.g. Crook, 1986; Menhofer *et al.*, 1997b). According to the linear theory for a two-dimensional sinusoidal wave propagating in a non-rotating, stably stratified, Boussinesq atmosphere, the vertical wave number m is related to the environmental conditions through the expression

$$m(z)^2 = l(z)^2 - k^2,$$

where

$$l(z)^2 = \frac{N(z)^2}{(U(z) - c)^2} - \frac{U_{zz}}{(U(z) - c)}$$

is the Scorer parameter, k is the horizontal wavenumber, z is the geometrical height, N is the Brunt-Väisäla frequency,

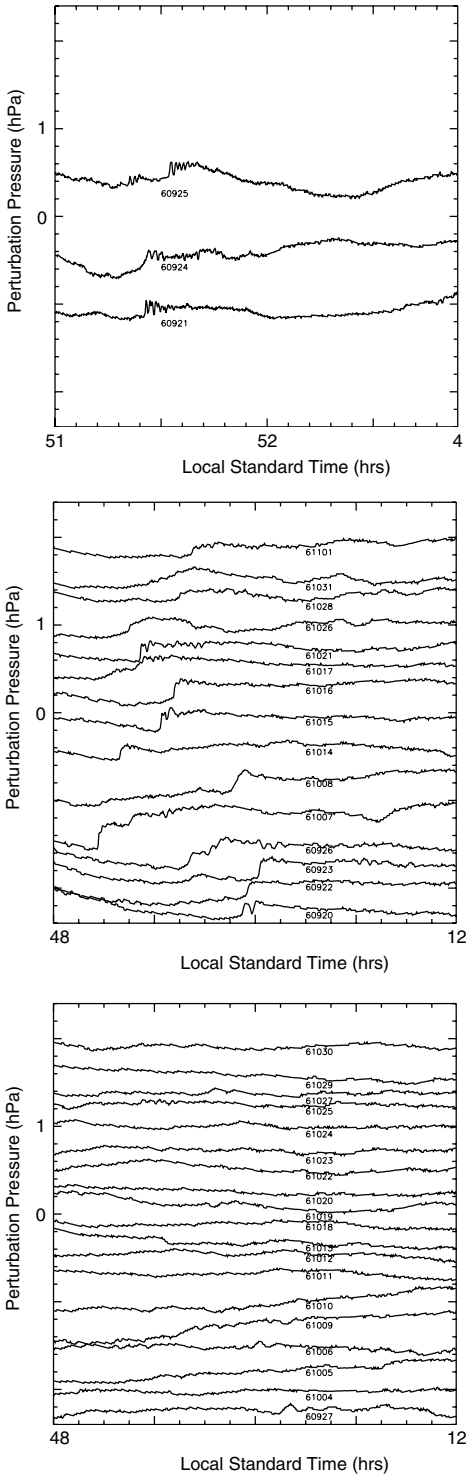

Figure 10. Perturbation pressure at Mornington Island. Top: easterlies from the Normanton sodar $< 10\ \mathrm{m\,s^{-1}}$. Days with solitary wave-like morning glories. Middle: easterlies from the Normanton sodar $> 10\ \mathrm{m\,s^{-1}}$. Days with jump-like morning glories. Bottom: days without morning glories. The date (year/month/day) is printed under each curve.

$U(z)$ is the component of the environmental flow normal to the wave and c is the horizontal phase speed. Small-amplitude gravity waves propagate vertically when m is real, but are evanescent when m is imaginary. Consequently, waves may be ducted when the environmental conditions, characterized by the vertical structure of the Scorer parameter, restrict their propagation to a layer.

One such configuration, thought to be important for the morning glory, is a stable surface-based layer permitting vertical propagation beneath a deep layer in which the waves are evanescent, preventing the appreciable loss of wave energy from the lower layer through upward propagation. Northeasterly morning glories propagate towards the southwest against an opposing low-level westerly (Figure 9) and hence $U(z) - c > 0$.

Crook (1988) discusses three configurations relevant to the morning glory. They are when $N(z)^2$ decreases with height, when $U(z)$ increases with height, or when U_{zz} changes sign from negative in the stable surface layer to positive aloft. One limitation of the data taken during GLEX III is that there are few observations of the thermodynamic structure of the atmosphere and, for this reason, it is not possible to calculate the Scorer parameter. However, previous studies of the region have shown that thermodynamic structure comprises a deep nearly neutral layer above a stably stratified surface layer, which is a few hundred metres deep (Menhofer *et al.*, 1997b; Smith *et al.*, 2006). Figure 9 shows that a strong low-level westerly jet immediately precedes the northeasterly surge on those days that develop solitary wave-like morning glories.

Although a low-level jet develops also on days that develop jump-like morning glories, it is several hours ahead of the easterly surge. This low-level jet enhances the propagation at the lowest levels by making $l(z)^2$ more positive, since $U_{zz}/(U(z) - c) < 0$. To the extent that the term $N(z)^2/(U(z) - c)^2$ is similar in the strong and weak collisions, the environment for the former case is more supportive of propagation than the latter case. In both cases, the flow reverses above about 500 m (Figure 9), which implies that $U_{zz}/(U(z) - c) > 0$. As argued by Crook, this change in sign makes $l(z)^2$ more negative and less supportive of propagation. Using radiosonde soundings taken in the southern Gulf, Menhofer *et al.* (1997b) showed that, although $U_{zz}/(U(z) - c)$ is mostly negative above the lowest few hundred metres, it is not uniformly so. Consequently, they concluded that the waves must be continuously forced; otherwise the waves would quickly attenuate as energy is lost through upward propagation.

7. Model Results

Prompted by the discussion in section 6, the relative roles of the collision and the waveguide structure in determining the structure and evolution of the morning glory is explored with two numerical simulations using MM5. The first simulation examines the generation and evolution of a morning glory from a weak collision on 19–20 September 2006, whereas the second examines the morning glory on 24–25 September 2006, which is an example of a strong collision. These are referred to as the weak-collision simulation and the strong-collision simulation, respectively.

Figure 12 shows vertical cross-sections of vertical motion, wind speed in the plane of the cross-section and potential temperature from the two simulations at about the time at which the east-coast and west-coast sea breezes collide over the Cape York Peninsula. The cross-sections are oriented northeast–southwest, which is normal to the resulting disturbance. In the weak-collision simulation, the normal flow is mostly strong and negative, which is in the direction of propagation of the east-coast sea breeze. There is only a shallow region of positive flow associated with the west-coast

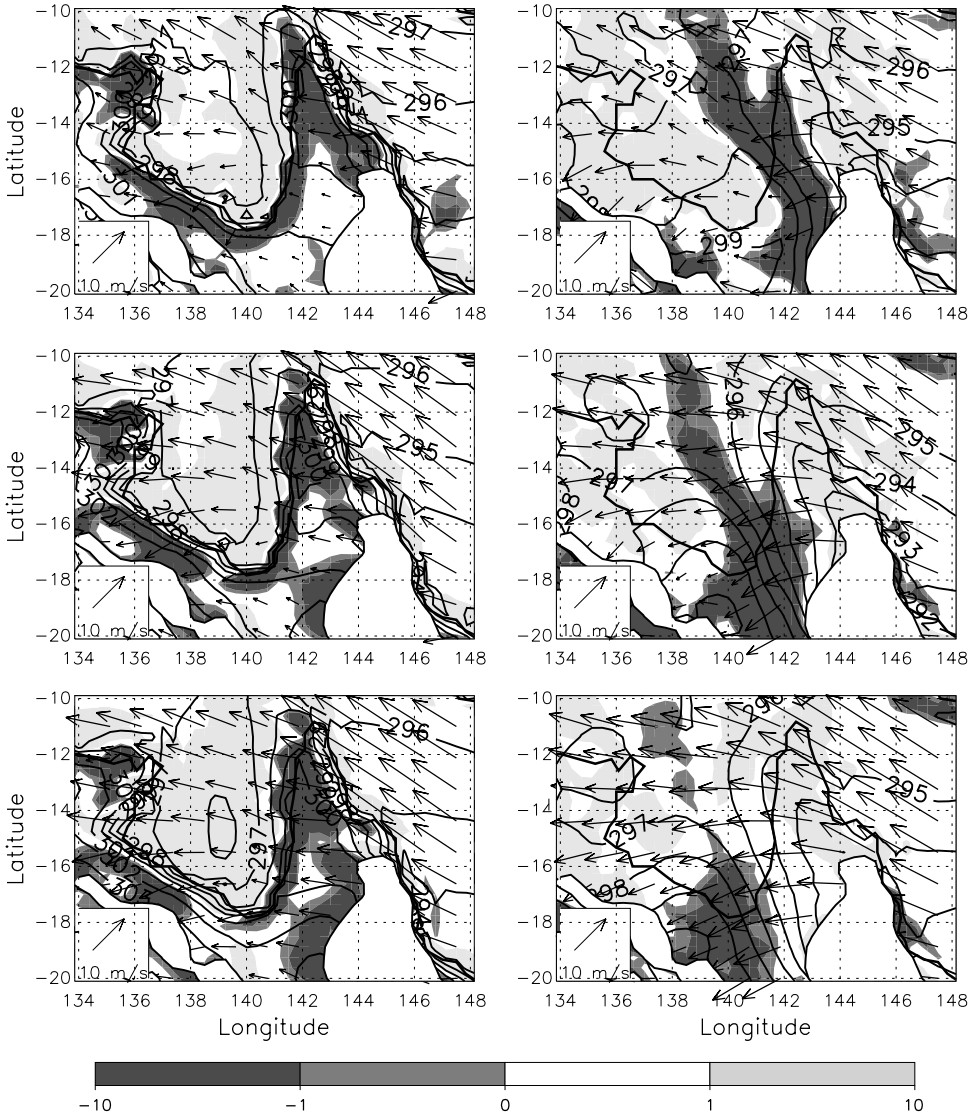

Figure 11. Composite LAPS 3 h forecasts at 950 mb showing convergence, horizontal winds and virtual temperature. Shading indicates divergence with units $\times 10^{-5}$ s^{-1}. The contour interval for virtual temperature is 1 K. Top row: days with solitary wave-like morning glories. Middle row: days with jump-like disturbances. Bottom row: days without disturbances. Left column: 1800 LST. Right column: 0600 LST. The blank areas enclosed with a solid dark line indicate topography above 250 m.

sea breeze. In contrast, in the strong-collision simulation, the flow is relatively symmetric, with comparable regions of positive and negative flow. The difference between the depth of the east-coast and west-coast sea breezes is much smaller also. Moreover, the vertical velocity is much larger than in the weak-collision simulation and a plume of potentially cold air is thrust upwards as the sea breezes collide.

Physically, the non-dimensional parameter $\mu = 2Nh/\pi U$ represents the ratio of the phase speed at which the small-amplitude waves propagate on the stable layer to a characteristic speed of the wind behind the leading edge of the east-coast sea breeze (Haase and Smith, 1989; Thomsen *et al.* 2009). In this expression, U is the typical value of the horizontal component of the wind in the cool air immediately behind the sea breeze front, N is the Brunt-Väisäla frequency in the stable layer ahead of the sea breeze and h is the depth of the stable layer. In the weak-collision simulation, $\mu = 0.6 \pm 0.3$, whereas in the strong-collision simulation $\mu = 1.6 \pm 0.9$. The uncertainty attached to the calculations of μ arises because of the difficulties in determining U, N and h in a time-varying, spatially complex flow. The likely errors in μ have been estimated graphically.

The weak-collision simulation appears to be supercritical, meaning that the speed of small-amplitude waves supported on the layer of cold air laid down by the west-coast sea breeze is smaller than the typical wind speed behind the east-coast sea breeze. In this case, the stable layer to the west of the east-coast sea breeze is comparatively shallow and weak, and the leading edge of the east-coast sea breeze becomes wave-like, although waves are unable to propagate ahead of the advancing cold air. In contrast, in the strong-collision simulation, the flow appears to be subcritical, meaning the stable layer provided by the west-coast sea breeze is sufficiently deep and strong to enable waves to propagate faster than the speed of the east-coast sea breeze. The east-coast sea breeze subsequently evolves into a large-amplitude solitary wave-like disturbance that propagates ahead of the advancing cold air.

From satellite observations, the wavelength of the morning glory waves is about 5 km in both events, while in both simulations the modelled wavelength is about 8

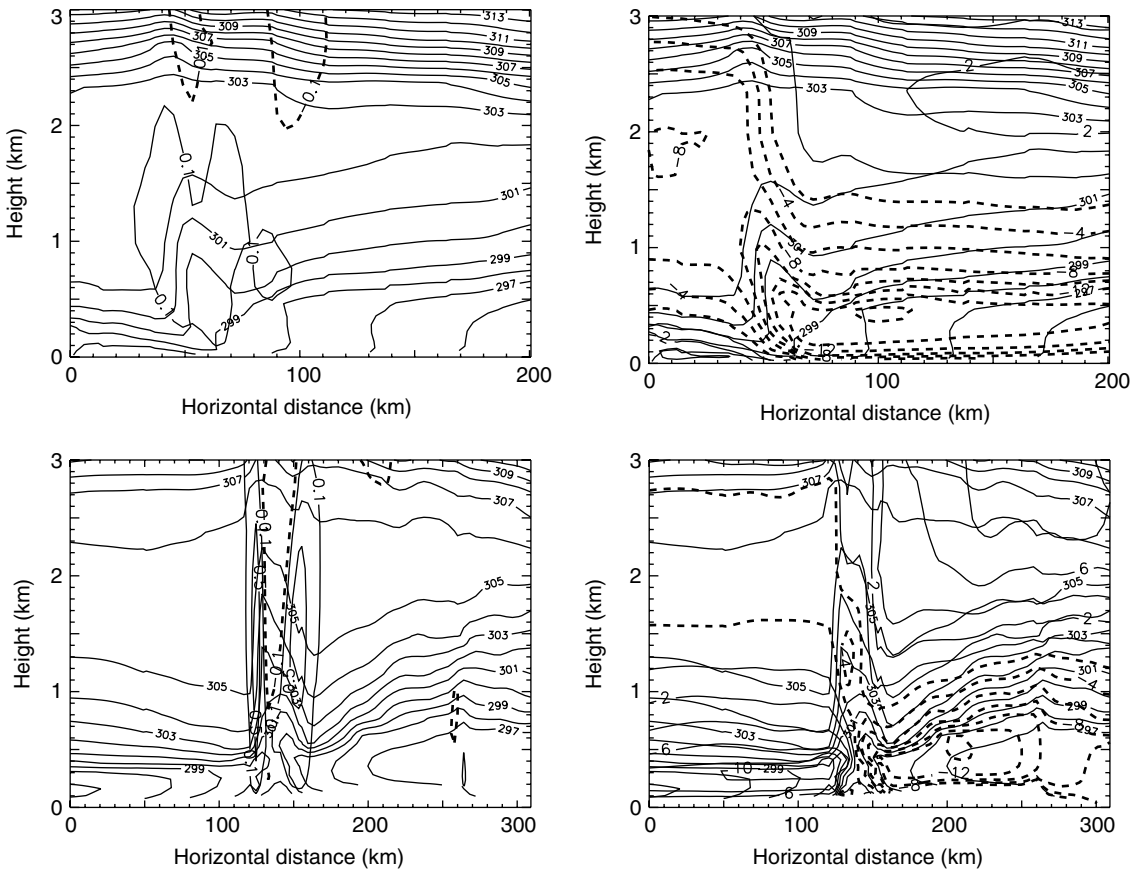

Figure 12. Vertical cross-sections from MM5 at the times at which the sea breezes meet over the Cape York Peninsula. The cross-section is oriented southwest–northeast, with positive horizontal distance pointing towards the northeast. Top row: weak-collision simulation at 2130 LST 19 September 2006. Bottom row: strong-collision simulation at 2030 LST 24 September 2006. Vertical motion (left column) and wind speed normal to the disturbance (right column). Background field is potential temperature in all panels. Wind speed contour interval 2 m s^{-1}. Negative contours dashed. Vertical motion contour levels (-1, -0.5, -0.1, 0.1, 0.5, 1) m s^{-1}. Potential temperature contour interval 1 K.

km. Hence the square of the wave number k^2 is about 1.6×10^{-6} m^{-2} and 0.6×10^{-6} m^{-2} in the observations and model, respectively. Figure 13 shows cross-sections of the Scorer parameter l^2 normal to the disturbances at the time of collision from the two simulations. In most of the domain, and certainly at low levels, $l^2 >> k^2$, implying that $m^2 \approx l^2$. Hence the Scorer parameter alone determines whether or not small-amplitude waves can propagate vertically. In the strong collision simulation, the environment into which the disturbance propagates ($x <$ 150 km) has the characteristics of a waveguide as l^2 is positive below about 400 m and negative or very weakly positive above. In contrast, l^2 is mostly negative or weakly positive in the downstream environment ($x < 60$ km) in the weak-collision simulation. Thus the interpretation that the weak collision is supercritical and the strong-collision simulation is subcritical is supported by the different patterns of Scorer parameter in the two simulations.

Vertical cross-sections of vertical motion, wind speed normal to the disturbance and potential temperature from the two simulations at about the time the morning glories arrive at Normanton are shown in Figure 14. As before, the cross-sections are oriented northeast–southwest. At this time the leading edge of the bore that develops in the weak-collision simulation is located at about $x = 80$ km. At this point the isentropes at low levels are displaced sharply upward by about 1200 m, and this displacement coincides with a strong updraught exceeding 1 m s^{-1}. Ahead of the bore (to the left) there is a relatively shallow stable layer roughly 300 m deep, whereas behind the bore (to the right) the atmosphere is almost well mixed through the lowest 400–500 m. The winds are strong and negative behind the bore, with the most negative exceeding 12 m s^{-1} in magnitude about 60 km to the rear. In contrast, the disturbance that develops in the strong-collision simulation is much weaker that in the weak collision simulation; the isentropic displacement and vertical motion at the leading edge are about half that in weak-collision simulation, and, compared with the latter, the stable layer ahead of the disturbance is much deeper and the stable stratification in the region behind the bore is stronger. Although the disturbance in the strong-collision simulation developed from an initially stronger collision than that in the weak-collision simulation, by the time it reaches Normanton it is much weaker, as characterized by the isentropic displacement and vertical motion.

8. Conclusions

During November and December 2005, the initiation of the NACL was documented principally from two sodars located at Weipa and Scherger Air Force Base. Aerosondes were used with limited success to take measurements of the wind, pressure, temperature and humidity. In September and October 2006, observations of southwestward-moving bore-like convergence lines over the southern part of the Gulf of Carpentaria region of northern Australia were documented at Normanton, Karumba and Mornington

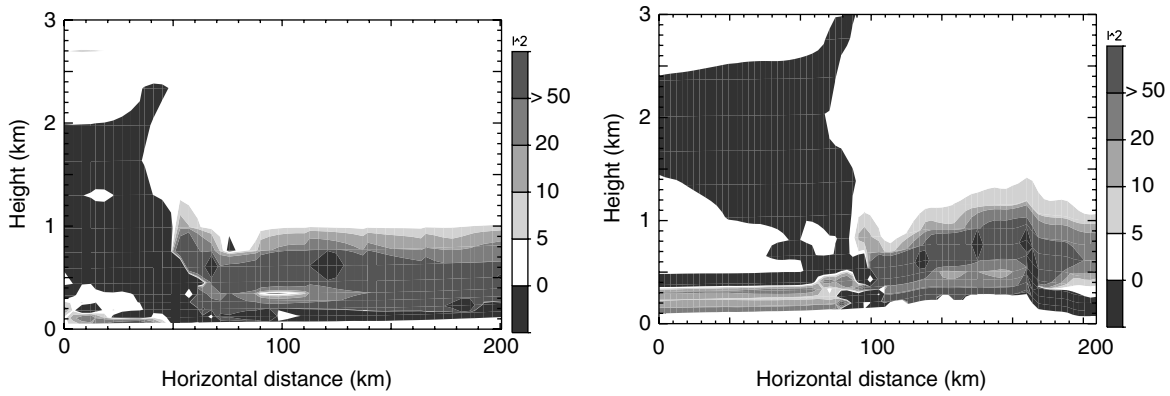

Figure 13. Vertical cross-sections of the Scorer Parameter (l^2) from MM5 when the sea breezes meet over the Cape York Peninsula. The cross-section is oriented southwest–northeast, with positive horizontal distance pointing towards the northeast. Left: weak-collision simulation at 2130 LST 19 September 2006. Right: strong-collision simulation at 2030 LST 24 September. Units for l^2 are 1×10^6 m^{-2}.

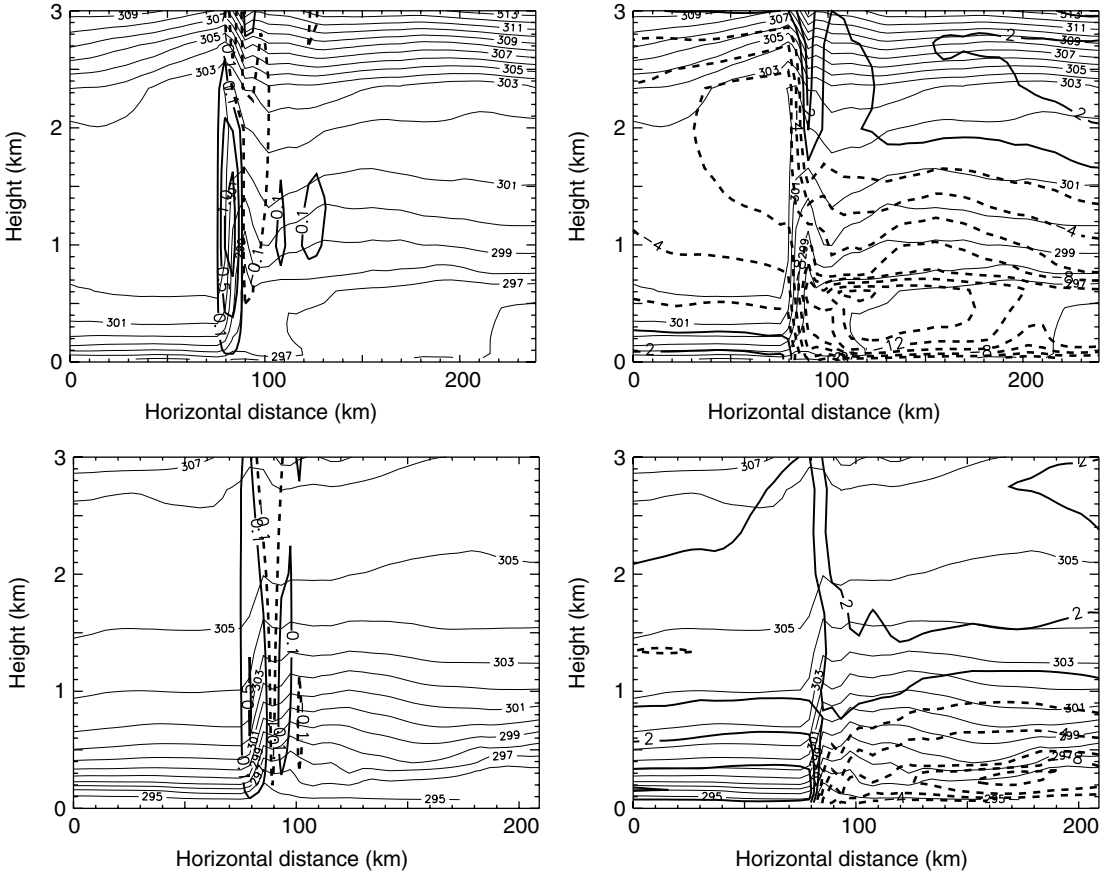

Figure 14. Vertical cross-sections from MM5 at the times at which the disturbance arrives at Normanton. The cross-section is oriented southwest–northeast, with positive horizontal distance pointing towards the northeast. Top row: weak-collision simulation at 0100 LST 20 September 2006. Bottom row: strong-collision simulation at 0530 LST 25 September 2006. Vertical motion (left column) and wind speed normal to the disturbance (right column). Background field is potential temperature in all panels. Wind speed contour interval 2 m s^{-1}. Negative contours are dashed. Vertical motion contour levels (-1, -0.5, -0.1, 0.1, 0.5, 1) m s^{-1}. Potential temperature contour interval 1 K.

Island. These observations were augmented with high-resolution simulations of two events from the southern phase to build a more complete picture of the initiation and propagation of the convergence lines that form in the region.

Composite time–height sections of the sodar winds at Weipa and Scherger were constructed, based on the speed of propagation of the NACLs, which was closely related to the maximum easterly component of the wind in the section between 0000 and 0900 LST. These composites showed that the degree of asymmetry between west-coast and east-coast sea breezes (as characterized by the wind field alone) depends on the strength of the background easterlies. No NACL developed on any day for which the maximum easterly in the composite was less than 5 m s^{-1}, whereas an NACL formed on every day on which the maximum easterly exceeded 5 m s^{-1}. At Normanton, composite time–height sections of the sodar winds showed that amplitude-ordered solitary waves developed downstream when the background easterlies were less than about 10 m s^{-1}. In contrast, either no jump or a single bore-like jump formed downstream when the background easterlies were greater than 10 m s^{-1} below

a height of 700 m (which is the depth of the boundary layer covered by the sodars). Taken together, the observations from the two field experiments, carried out at opposite ends of the Cape York Peninsula, suggested that strong easterlies favour the formation of the NACL in the northwestern part of the peninsula, whereas weak easterlies favour the formation of the morning glory in the southwest.

The numerical simulations showed that the structure of the disturbance produced depends on the strength of the collision between the asymmetric sea breezes, which in turn depends on the strength of the background easterlies. When the easterlies are comparatively weak, the sea breezes are relatively symmetric and their collision relatively violent. These results suggest that this case is subcritical in the sense that the stable layer provided by the west-coast sea breeze is sufficiently deep and strong to enable waves to propagate faster than the speed of the the east-coast sea breeze. The disturbance subsequently evolves into a series of amplitude-ordered solitary waves that runs ahead of the east-coast sea breeze. In contrast, when the background easterlies are stronger, the sea breezes are asymmetric. In this case, the collision is comparatively gentle, with the east-coast sea breeze simply surmounting the west-coast sea breeze and running across the top of the cold air. These results suggest that this case is supercritical in the sense that the speed of small-amplitude waves supported on the layer of cold air advected onshore by the west-coast sea breeze is smaller than the typical wind speed behind the east-coast sea breeze.

The observations and numerical results support the previous theoretical predictions, and are important as they clarify the role of the synoptic-scale flow in the formation (or not) of the most common types of propagating convergence lines in the region.

Acknowledgements

We are grateful to the Australian Research Council (DP0558793) and the German Research Council (DFG) for their financial support. We would like to thank also the Australian Bureau of Meteorology for providing the LAPS data and the European Centre for Medium Range Weather Forecasts for the analyses from which MM5 was run.

References

Arnup SJ, Reeder MJ. 2007. The diurnal and seasonal variation of airmass boundaries in the Australian region. *Mon. Weather Rev.* **135**: 2995–3008.

Arnup SJ, Reeder MJ. 2009. The structure and evolution of the northern Australian dryline. *Aust. Meteorol. Ocean. J.* **58**: 215–231.

Christie DR. 1992. The morning glory of the Gulf of Carpentaria: a paradigm for nonlinear waves in the lower atmosphere. *Aust. Meteorol. Mag.* **41**: 21–60.

Clarke RH. 1983a. Fair weather nocturnal wind surges and atmospheric bores. Part I: Nocturnal wind surges. *Aust. Meteorol. Mag.* **31**: 133–145.

Clarke RH. 1983b. Fair weather nocturnal wind surges and atmospheric bores. Part II: Internal atmospheric bores in northern Australia. *Aust. Meteorol. Mag.* **31**: 147–160.

Clarke RH. 1984. Colliding sea-breezes and the creation of internal atmospheric bore waves: two dimensional numerical studies. *Aust. Meteorol. Mag.* **32**: 207–226.

Clarke RH, Smith RK, Reid DG. 1981. The morning glory of the Gulf of Carpentaria: an atmospheric undular bore. *Mon. Weather Rev.* **109**: 1726–1750.

Crook NA. 1986. The effect of ambient stratification and moisture on the motion of atmospheric undular bores. *J. Atmos. Sci.* **43**: 171–181.

Crook NA. 1988. Trapping of low-level internal gravity waves. *J. Atmos. Sci.* **45**: 1533–1541.

Deslandes R, Reeder MJ, Mills G. 1999. Synoptic analyses of a subtropical cold front observed during the 1991 Central Australian Fronts Experiment. *Aust. Meteorol. Mag.* **48**: 87–110.

Dudhia J. 1989. Numerical study of convection observed during the winter monsoon experiment using a mesoscale two-dimensional model. *J. Atmos. Sci.* **46**: 3077–3107.

Dudhia J. 1993. A nonhydrostatic version of the Penn State-NCAR mesoscale model: Validation tests and simulation of an Atlantic cyclone and cold front. *Mon. Weather Rev.* **121**: 1493–1513.

Garand L. 1983. Some improvements and complements to the infrared emissivity algorithm including a parameterization of the absorption in the continuum region. *J. Atmos. Sci.* **40**: 230–243.

Goler RA, Reeder MJ. 2004. The generation of the morning glory. *J. Atmos. Sci.* **61**: 1360–1376.

Goler RA, Reeder MJ, Smith RK, Arnup S, Richter H, Keenan T, May P. 2006. Low-level convergence lines over northern Australia. I. The North Australian Cloud Line. *Mon. Weather Rev.* **134**: 3092–3108.

Grell GA, Dudhia J, Stauffer D. 1995. A description of the 5th generation Penn State/NCAR mesoscale model (MM5). *Technical Report 398*, NCAR.

Haase SP, Smith RK. 1989. The numerical simulation of atmospheric gravity currents. Part II: Environments with stable layers. *Geophys. Astrophys. Fluid Dyn.* **46**: 35–51.

Hong SY, Pan HL. 1996. Nonlocal boundary layer vertical diffusion in a medium-range forecast model. *Mon. Weather Rev.* **124**: 1322–2399.

Jackson GE, Smith RK, Spengler T. 2002. The numerical prediction of cloud lines over northern Australia. *Aust. Meteorol. Mag.* **51**: 13–24.

May PT. 1995. The Australian nocturnal jet and diurnal variations of boundary layer winds over Mt Isa in north-eastern Australia. *Q. J. R. Meteorol. Soc.* **121**: 987–1003.

Menhofer A, Smith RK, Reeder MJ, Christie DR. 1997a. The bore-like character of three morning glories observed during the Central Australian Fronts Experiment. *Aust. Meteorol. Mag.* **46**: 277–285.

Menhofer A, Smith RK, Reeder MJ, Christie DR. 1997b. Morning glory disturbances and the environment in which they propagate. *J. Atmos. Sci.* **54**: 1712–1725.

Noonan JA, Smith RK. 1986. Sea breeze circulations over Cape York Peninsula and the generation of Gulf of Carpentaria cloud line disturbances. *J. Atmos. Sci.* **43**: 1679–1693.

Noonan JA, Smith RK. 1987. Generation of north Australian cloud lines and the 'morning glory'. *Aust. Meteorol. Mag.* **35**: 31–45.

Puri K, Dietachmayer GS, Mills GA, Davidson NE, Bowen RA, Logan LW. 1998. The new BMRC Limited Area Prediction Scheme, LAPS. *Aust. Meteor. Mag.* **47**: 203–223.

Reeder MJ, Smith RK. 1998. Mesoscale meteorology. In *Meteorology of the Southern Hemisphere*, Karoly DJ, Vincent DG (eds). American Meteorological Society: Boston, MA; 201–241.

Reeder MJ, Christie DR, Smith RK, Grimshaw R. 1995. Interacting morning glories over northern Australia. *Bull. Am. Meteorol. Soc.* **76**: 1165–1171.

Reeder MJ, Smith RK, Deslandes R, Tapper NJ, Mills GA. 2000. Subtropical fronts observed during the 1996 Central Australian Fronts Experiment. *Aust. Meteorol. Mag.* **49**: 181–200.

Smith RK, Reeder MJ, Tapper NJ, Christie DR. 1995. Central Australian cold fronts. *Mon. Weather Rev.* **123**: 19–38.

Smith RK, Reeder MJ, May P, Richter H. 2006. Low-level convergence lines over northern Australia. II. Southerly disturbances. *Mon. Weather Rev.* **134**: 3109–3124.

Stephens GL. 1978. Radiation profiles in extended water clouds. II: Parameterization schemes. *J. Atmos. Sci.* **35**: 2123–2132.

Stephens GL, Ackerman SA, Smith EA. 1984. A shortwave parameterization revised to improve cloud absorption. *J. Atmos. Sci.* **41**: 687–690.

Thomsen GL, Smith RK. 2006. Simulations of low-level convergence lines over northeastern Australia. *Q. J. R. Meteorol. Soc.* **132**: 691–707.

Thomsen GL, Smith RK. 2008. The importance of the boundary layer parameterization in the prediction of low-level convergence lines. *Mon. Weather Rev.* **136**: 2173–2185.

Thomsen GL, Reeder MJ, Smith RK. 2009. Modelling the subtropical cold fronts and bores observed during the Central Australian Fronts Experiment. *Q. J. R. Meteorol. Soc.* **135**: 395–411.

Weinzierl B, Smith RK, Reeder MJ, Jackson G. 2007. MesoLAPS predictions of low-level convergence lines over northeastern Australia. *Weather Forecast.* **22**: 910–927.

